

Sophisticated Construction of Au Islands on Pt–Ni: An Ideal Trimetallic Nanoframe Catalyst

Yuen Wu,[†] Dingsheng Wang,[†] Gang Zhou,[‡] Rong Yu,[§] Chen Chen,^{*,†} and Yadong Li^{*,†}

[†]Department of Chemistry, Tsinghua University, Beijing 100084, People's Republic of China

[‡]State Key Laboratory of Chemical Resource Engineering, Beijing University of Chemical Technology, Beijing 100029, People's Republic of China

[§]Beijing National Center for Electron Microscopy, School of Materials Science and Engineering, Tsinghua University, Beijing 100084, People's Republic of China

S Supporting Information

ABSTRACT: We have developed a priority-related chemical etching method to transfer the starting Pt–Ni polyhedron to a nanoframe. Utilizing the lower electronegativity of Ni in comparison to Au atoms, in conjunction with the galvanic replacement of catalytically active Au to Ni tops, a unique Au island on a Pt–Ni trimetallic nanoframe is achieved. The design strategy is based on the structural priority mechanism of multimetallic nanocrystals during the synthesis and thus can be generalized to other analogous metal–bimetallic nanocrystal combinations (such as Pd and Cu islands on Pt–Ni nanoframes), which is expected to pave the way for the future development of efficient catalysts.

Having a lower coordination number, corner and edge atoms, rather than those at the flat surface, are generally the preferred sites to activate most important catalytic reactions due to the lower activation energy and altered electronic structure.^{1,2} Nanostructures with open surface features such as high-index facet,³ concave surface,⁴ and porous structure^{5,6} have provoked ever-increasing attention in the field of catalysis due to their exceptional catalytic properties. Metallic nanoparticles (NPs) with a nanoframe structure, in which edges are joined together at specific corners to create a skeletal frame, can harvest the costly materials and supply the three-dimensional molecular accessibility, thus serving as an ideal model catalyst to satisfy the ultimate goal of NP catalysis. Several pioneering works have been established to obtain this unique nanostructure, such as monometallic Au^{7,8} and bimetallic Au–Ag⁹ and Pt–Cu nanoframes,¹⁰ with outstanding physical and chemical properties. Very recently, Chen et al. observed that a Pt₃Ni rhombic dodecahedral nanoframe composed of 24 edges and 14 corners enables the maximum utilization of Pt by a three-dimensional accessible surface.¹¹ The fascinating geometric and electronic effects induced by the nanosegregated Pt-skin surface confer a substantial improvement in activity toward the oxygen reduction reaction to this unique nanoframe catalyst. Because of this progress, designing multicentered and multifunctional nanostructures with high efficiency is currently becoming a promising area. In this report, a previously unknown sequential strategy is exploited to construct a novel trimetallic nanoframe catalyst. The corners of Pt–Ni nanoframes can be sophisti-

catedly anchored with Au islands by galvanic replacement, masterly utilizing the highly active top Ni atoms. Afterward, structural priority related chemical etching is used to carefully regulate the corrosion of Ni and rearrangement of Pt atoms to achieve the nanosegregated Pt-skin edges. This ingenious design not only guarantees the major proportion of versatile active sites but also directly supports synergistic effects between Au islands and Pt–Ni edges, which will extend our ability to improve activity, selectivity, and durability. We believe such previously unreported integration of selective galvanic replacement and priority-related chemical etching gives us the key to open up a new trimetallic family of nanoframes with surface-decorating atoms for the selection of ideal NP catalysts.

We first present an efficient method for synthesizing novel bimetallic Pt–Ni nanoframes by transforming truncated octahedral Pt–Ni alloy particles through a priority-related chemical etching process.¹² Figure 1a shows both transmission electron microscope (TEM) and high-resolution TEM (HRTEM) (inset) images of the truncated octahedral PtNi₃ NPs. After dimethylglyoxime was applied to a suspension of the PtNi₃ NPs, the Ni could be gradually etched from the PtNi₃ alloy by oxidative etching. Figure 1b reveals that most of the obtained NPs retained their original symmetry and showed a narrow size distribution (average size of 12.5 ± 1.5 nm). Examination of the HRTEM image shown in Figure 1c indicates that each particle possesses an eroded hollow frame. The high-angle annular dark-field scanning transmission electron microscope (HAADF-STEM) micrograph (Figure 1d) indicates that parts of the framework are much brighter than the other region of the particles, further demonstrating the presence of a nanoframe structure. The structural evolution of the particles from the parent PtNi₃ polyhedrons to final products was accompanied by a variation in elemental distribution. According to the elemental maps shown in Figure 1d and cross-sectional compositional line profiles of a truncated octahedral PtNi₃ particle (Figure S2, Supporting Information), the distribution of Ni in the starting PtNi₃ particles showed a slight enrichment in the central region, whereas a homogeneous distribution of Pt throughout the entire particle was observed. After chemical etching, the as-obtained truncated octahedral

Received: June 14, 2014

Published: August 5, 2014

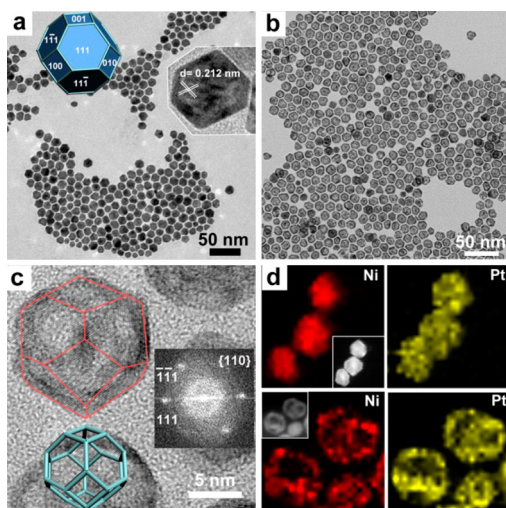


Figure 1. (a) TEM and HRTEM images of truncated octahedral PtNi_3 . The inset shows the ideal model of a truncated octahedron. (b) TEM and (c) HRTEM images of the Pt_3Ni nanoframe (the insets in (c) are the fast Fourier transform patterns and corresponding ideal model of the nanoframe). (d) HAADF-STEM image and corresponding elemental maps (Pt (yellow) and Ni (red)).

nanoframes retained an overall 36 edges of the truncated octahedron, in which both Pt and Ni exhibited homogeneous distributions, implying that the final product formed an alloy phase.

It is undoubtedly very important to understand the etching-dominated fabrication methods of alloy NPs with well-designed shapes. For this purpose, we investigated the surface-dependent etching processes and mechanisms of PtNi_3 NPs by density functional theory calculations, crystal structures, and etching reaction analyses. A thermodynamic viewpoint showed that the dissolution rate of Ni atoms is faster than that of Pt atoms, following the order edge > (110) \approx (100) > (111) surfaces (see the Supporting Information for details and Figure 2). The proposed processes involved in the shape evolution of truncated octahedral PtNi_3 NPs are schematically illustrated in Figure 2. As for octahedral PtNi_3 NPs,¹² the etching of (111) surfaces proceeded in a layer-by-layer removal manner (Figure 2a), which in principle yielded a Pt-rich concave solid structure. However, the open (100) surfaces exhibited a distinctly different etching process and mechanism because of alternate stacking of full Ni and Pt–Ni alternately in the structure. More precisely, after Ni dissolution, the surface Pt aggregated, driven by the near-neighbor bonding to form a “porous Pt shell”. It inhibited the binding between exposed subsurface Ni and dimethylglyoxime, which is a crucial stage of oxidative etching of Pt–Ni alloy.¹² The subsequent etching process was unilaterally controlled by outward diffusion of Ni^{2+} from NPs, accompanying the inward flow of vacancies, through the pores of the inert Pt shell (Figure 2b). It followed a mechanism analogous to the Kirkendall effect.^{13,14} As the reaction proceeded deeper into the Ni center, the etching rate should increase significantly, which allowed mobility of vacancies and growth and coalescence of small cavities. When reaching the Kirkendall hole, the etching of {111} surfaces would open the NPs (Figure 2c). Meanwhile, growing stress-corrosion cracks would in time decompose the Pt-segregated layers, which was not present in the hollowing of metals.¹⁴ Following the step-induced/terrace-assisted growth mechanism of alloy NPs,¹⁵ the

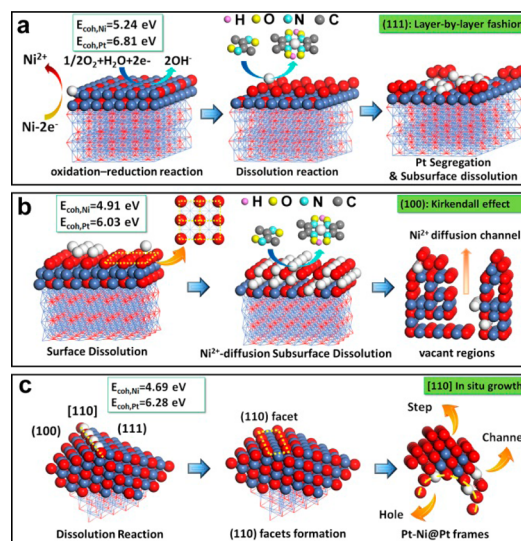


Figure 2. Schematic illustration of the proposed etching mechanism of truncated octahedral PtNi_3 NPs from DFT calculations, combined with crystal structure and etching reaction analysis: (a, b) etching processes of {111} and {100} surfaces; (c) formation of [110] frame. Red, blue, and white balls correspond to Pt and Ni atoms and Ni^{2+} , respectively.

decomposed Pt atoms would readily occupy the Ni vacancies which formed earlier at the edges by migration,¹⁶ thereby exhibiting the radial thickening of the Pt–Ni@Pt frame with progressing time (Figure 2c). The nonsusceptibility of Pt to dimethylglyoxime solution¹⁷ and strong Pt–Pt bonds allowed Pt-protected frames to be retained as far as possible after the etching. These were in agreement with the experimental observations. Therefore, it is confirmed that the existence of open {100} surfaces and Kirkendall effects stemming from distinct diffusion coefficients of Ni and Pt are the major reasons truncated octahedral PtNi_3 could yield the hollow structure by chemical etching.

To gain comprehensive insights into the structure–activity relationship of a catalyst, based on an understanding of priority-related chemical etching, we designed an experiment simultaneously involving the effects of morphology and composition within a single sample. We also chose truncated octahedral PtNi_3 particles as the starting polyhedrons for depositing Au islands on Pt–Ni nanoframe hybrid structures by a sequential process. The structural evolution from truncated octahedral PtNi_3 , to Au on PtNi_3 , to Au on PtNi, and finally to Au on Pt_3Ni is illustrated in Figure 3. The first step of this process starts with a mild galvanic replacement between Au(III) and Ni(0), which mainly results from the greater electro-negativity of Au with respect to Ni. When the PtNi_3 truncated octahedrons with sharp corners react with a trace amount of HAuCl_4 solution, the replacement initiates local low-coordination sites owing to their high surface free energy.¹⁸ It is reasonable to anticipate that the replacement reaction prevails at corners rather than edges and faces, which guarantees that Au(III) ions have a greater probability oxidizing Ni atoms at corners, thereby forming top Au(0) atoms in situ. As the reaction proceeds, the Au atoms form isolated clusters or very small NPs at the top of the original truncated octahedron. The HRTEM image shown in Figure 3b indicates that the core of the particles remained a truncated octahedron, and the protruding parts, which are much darker, suggest that the

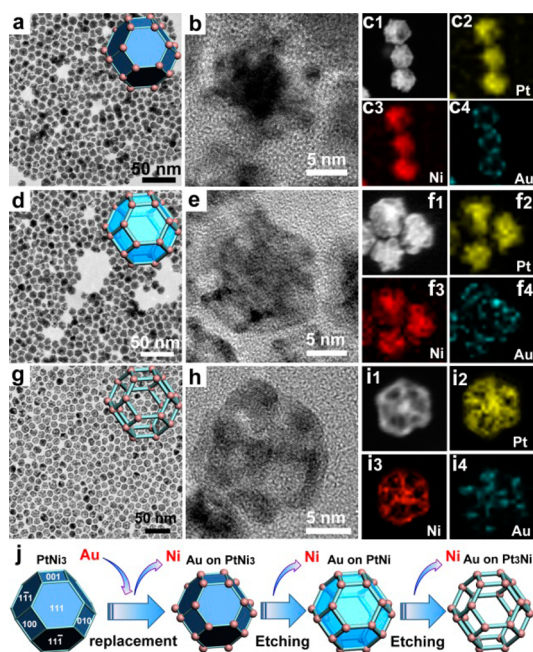


Figure 3. TEM images of (a) 10% Au on PtNi₃, (d) 10% Au on PtNi, and (g) 10% Au on Pt₃Ni. HRTEM images of (b) 10% Au on PtNi₃, (e) 10% Au on PtNi, and (h) 10% Au on Pt₃Ni. EDS elemental mapping images of (c) 10% Au on PtNi₃, (f) 10% Au on PtNi, and (i) 10% Au on Pt₃Ni. (j) Schematic illustration of the structural change from the truncated octahedral PtNi₃ to trimetallic hybrid Au islands on the Pt₃Ni nanoframe.

heavier gold islands clustered around the core. To further elucidate the nature of this unique hybrid structure, we also carried out EDS elemental mapping measurements. Unlike the homogeneous distribution of Pt and Ni throughout each particle (Figure 3c2 and 3c3), the turquoise dots in Figure 3c4 clearly indicate the existence of isolated Au islands. The second step after replacement was the chemical etching process. With an increase in the amount of etchant, the compositions of these hybrid structures continued to evolve from 10% Au on PtNi₃, to 10% Au on PtNi, to 10% Au on Pt₃Ni, which was consistent with the morphological transformation of the Pt–Ni cores from truncated octahedrons to truncated octahedral nanoframes. Figure 3 shows TEM images of the samples at three different stages, which demonstrated a morphological yield of up to 95%.

Very recently, it was demonstrated that a third metal can indeed affect the adsorption energy of an adsorbed substrate such as CO on the bimetallic surface by the direct electronic coupling between different domains.^{19–21} As shown in Figure 4a, the Pt 4f_{7/2} and 4f_{5/2} peaks of the Pt₃Ni frames corresponded to Pt⁰. Similarly, the Ni 2p_{3/2} peak could be assigned to Ni⁰ (Figure S12, Supporting Information). Comparatively, an apparent decrease in binding energy was observed for Au islands on the Pt₃Ni frame structures. The results strongly indicate that the Au islands on the Pt–Ni frame do have electron communication with Pt and Ni, which is in reasonable agreement with our DFT calculations, where electrons were transferred from Au islands to Pt₃Ni frames (see inset of Figure 4a). In particular, some exposed Au at the interface was reduced to electron-deficient δ⁺, an indication of synergistic effects, which might favor the diversity or/and selectivity of catalytic reactions. The hydrogenation reaction of aromatic nitro groups is an important industrial process. However, when the reactant molecules consist of other

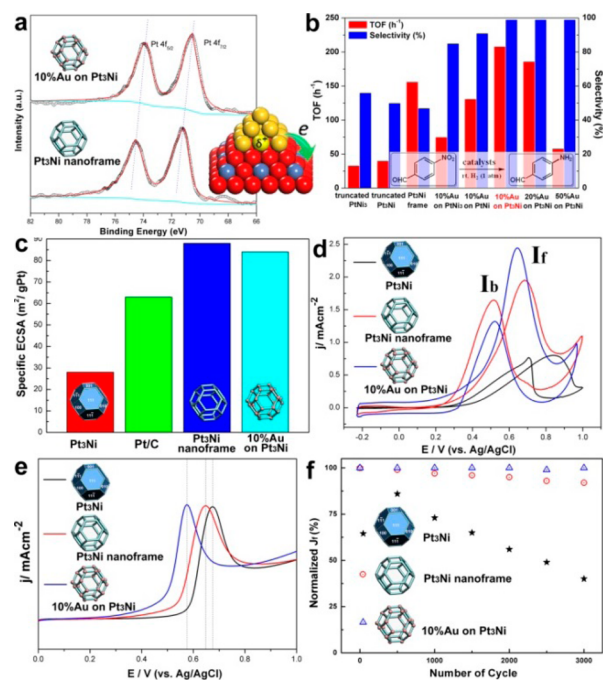


Figure 4. (a) Pt 4f XPS spectra of Pt₃Ni frame and 10% Au on Pt₃Ni nanoframe (the inset illustrates the charge transfer from Au islands to Pt₃Ni frames in trimetallic systems; red, blue and yellow balls correspond to Pt, Ni, and Au, respectively). (b) Selectivity and TOFs of 4-nitrobenzaldehyde hydrogenation with different catalysts as a function. (c) Specific ECSAs for different catalysts recorded in 0.1 M HClO₄. (d) Cyclic voltammograms of methanol oxidation on different catalysts in 0.1 M HClO₄ containing 1 M MeOH. (e) Cyclic voltammograms of CO stripping on different catalysts recorded in 0.1 M HClO₄ with a scan rate of 100 mV s⁻¹. (f) Loss of peak current density in a forward scan as a function of cycling numbers.

reducible groups such as C=C and C=O, the nitro groups are difficult to reduce in a selective manner.²² Utilizing the hydrogenation of 4-nitrobenzaldehyde as a model probe reaction, we could evaluate the catalytic behavior of truncated octahedral PtNi₃ NPs and Pt₃Ni, Pt₃Ni nanoframes and hybrid Au on Pt–Ni with respect to both activity and selectivity. As shown in Figure 4b, due to their larger surface area, the Pt₃Ni frames exhibited a higher activity turnover frequency (TOF) than the truncated octahedral PtNi₃ and Pt₃Ni particles, whereas much lower selectivity was measured (46%). The Pt–Ni alloys presented a mixture of two reduction products (4-aminobenzaldehyde and 4-nitrobenzyl alcohol). With small amounts of Au islands decorated on the Pt₃Ni frames, the Au on Pt–Ni showed an even better initial activity turnover frequency (TOF) than the Pt₃Ni frames and almost 100% selectivity toward 4-aminobenzaldehyde. It is not surprising that the improved selectivity resulted from the selective adsorption of nitro groups on the surface of Au corners,²³ while the enhanced activity TOF might be attributed to localized electron communication between the Au corners and Pt₃Ni edges. However, an increase in the amount of Au did not cause a further enhancement in activity but instead a significant decay. It is possible that the overgrowth of Au islands may occur on the NPs, blocking the reactive sites and thereby hindering the contact between the substrate and inner Pt₃Ni core.

Furthermore, we used the optimal amount of Au on the Pt₃Ni catalysts (10%) to further study the particles' catalytic

properties toward the electro-oxidation of methanol. Given the charge formed during the hydrogen adsorption/desorption process after the correction for double-layer formation, the nanoframe catalysts exhibited notably larger electrochemically active surface areas than those of the Pt₃Ni truncated octahedrons (Figure 4c). Similarly, the nanoframes also exhibited excellent electrocatalytic activity toward the electro-oxidation of methanol (Figure 4d). Remarkably, the doping of Au islands on the Pt₃Ni nanoframes could significantly increase the I_f/I_b ratio (I_f and I_b are the forward and backward current densities, respectively). This result indicates that the presence of Au islands can facilitate the oxidation of methanol via a more effective route and prevent the generation of poisoning species such as CO.²⁴ To confirm this inference, we further carried out CO stripping experiments. As clearly shown in Figure 4e, 10% Au on the Pt₃Ni nanoframes allowed for a higher CO-resistant activity in comparison with that of other catalysts. In addition, this hybrid trimetallic nanoframe exhibited outstanding electrochemical durability (Figure 4f), which is derived from the surface decoration of Au and the corresponding CO-resistant activity. For the truncated octahedral Pt–Ni particles, a substantial specific activity loss was observed in cycling tests, which can be ascribed to the dissolution of the Pt surface and the CO poisoning effect on the oxidation/reduction process.²⁵ In contrast, high catalytic activity was retained with 10% Au on the Pt₃Ni nanoframe catalysts even after 3000 cycles. As mentioned previously, the skin surface of the nanoframes obtained by chemical etching is rich in Pt, which should strengthen the stability of this open structure and prevent the dissolution of Pt.²⁶ Moreover, the synergistic effect between the Au islands and Pt–Ni frame should weaken the binding of adsorbed and poisonous intermediates on the particle surface,²⁷ thus facilitating the durability of this ternary hybrid nanoframe catalyst.

In summary, a novel chemical etching strategy for fabricating Pt₃Ni nanoframes from a parent Ni-rich Pt–Ni alloy was developed in this study. The underlying mechanism for the formation of the nanoframes through chemical etching was proposed according to a theoretical study and supported by experimental observations. We further anticipate that the experiments revealing the effects of morphology and composition simultaneously in a sample will initiate attempts to comprehensively understand the structure–activity relationship of similar catalysts for commercial applications.

■ ASSOCIATED CONTENT

■ Supporting Information

Text, figures, and tables giving details of trimetallic Pt–Ni nanoframe control experimental synthesis, characterization data, and their catalytic reactions and detailed information about DFT calculations. This material is available free of charge via the Internet at <http://pubs.acs.org>.

■ AUTHOR INFORMATION

Corresponding Authors

*E-mail for C.C.: cchen06@mails.tsinghua.edu.cn.

*E-mail for Y.L.: yldli@mail.tsinghua.edu.cn.

Notes

The authors declare no competing financial interest.

■ ACKNOWLEDGMENTS

This work was supported by the State Key Project of Fundamental Research for Nanoscience and Nanotechnology (2011CB932401 and 2011CBA00500), National key Basic Research Program of China (2012CB224802), and the National Natural Science Foundation of China (Grant Nos. 21221062, 21171105, 21322107, and 21131004). This work made use of the resources of the Beijing National Center for Electron Microscopy.

■ REFERENCES

- (1) Liu, Z.-P.; Hu, P. *J. Am. Chem. Soc.* **2003**, *125*, 1958.
- (2) Lebedeva, N.; Koper, M.; Feliu, J.; Van Santen, R. *J. Phys. Chem. B* **2002**, *106*, 12938.
- (3) Quan, Z.; Wang, Y.; Fang, J. *Acc. Chem. Res.* **2012**, *46*, 191.
- (4) Cui, C.; Gan, L.; Heggen, M.; Rudi, S.; Strasser, P. *Nat. Mater.* **2013**, *12*, 765.
- (5) Tüysüz, H.; Hwang, Y. J.; Khan, S. B.; Asiri, A. M.; Yang, P. *Nano Res.* **2013**, *6*, 47.
- (6) Snyder, J.; McCue, I.; Livi, K.; Erlebacher, J. *J. Am. Chem. Soc.* **2012**, *134*, 8633.
- (7) Sun, Y.; Xia, Y. *Science* **2002**, *298*, 2176.
- (8) McEachran, M.; Keogh, D.; Pietrobon, B.; Cathcart, N.; Gourevich, I.; Coombs, N.; Kitaev, V. *J. Am. Chem. Soc.* **2011**, *133*, 8066.
- (9) Hong, X.; Wang, D.; Cai, S.; Rong, H.; Li, Y. *J. Am. Chem. Soc.* **2012**, *134*, 18165.
- (10) Xia, B. Y.; Wu, H. B.; Wang, X.; Lou, X. W. *J. Am. Chem. Soc.* **2012**, *134*, 13934.
- (11) Chen, C.; Kang, Y.; Huo, Z.; Zhu, Z.; Huang, W.; Xin, H. L.; Snyder, J. D.; Li, D.; Herron, J. A.; Mavrikakis, M.; Chi, M.; More, K. L.; Li, Y.; Markovic, N. M.; Somorjai, G. A.; Yang, P.; Stamenkovic, V. R. *Science* **2014**, *343*, 1339.
- (12) Wu, Y.; Wang, D.; Niu, Z.; Chen, P.; Zhou, G.; Li, Y. *Angew. Chem., Int. Ed.* **2012**, *124*, 12692.
- (13) Yin, Y.; Rioux, R. M.; Erdonmez, C. K.; Hughes, S.; Somorjai, G. A.; Alivisatos, A. P. *Science* **2004**, *304*, 711.
- (14) González, E.; Arbiol, J.; Puentes, V. F. *Science* **2011**, *334*, 1377.
- (15) Wu, Y.; Wang, D.; Chen, X.; Zhou, G.; Yu, R.; Li, Y. *J. Am. Chem. Soc.* **2013**, *135*, 12220.
- (16) Kellogg, G.; Feibelman, P. J. *Phys. Rev. Lett.* **1990**, *64*, 3143.
- (17) Gazda, D. B.; Fritz, J. S.; Porter, M. D. *Anal. Chim. Acta* **2004**, *508*, 53.
- (18) Zhang, H.; Watanabe, T.; Okumura, M.; Haruta, M.; Toshima, N. *Nat. Mater.* **2011**, *11*, 49.
- (19) Zhang, S.; Guo, S.; Zhu, H.; Su, D.; Sun, S. *J. Am. Chem. Soc.* **2012**, *134*, 5060.
- (20) Wang, D. Y.; Chou, H. L.; Lin, Y. C.; Lai, F. J.; Chen, C. H.; Lee, J. F.; Hwang, B. J.; Chen, C. C. *J. Am. Chem. Soc.* **2012**, *134*, 10011.
- (21) Tan, Y.; Fan, J.; Chen, G.; Zheng, N.; Xie, Q. *Chem. Commun.* **2011**, *47*, 11624.
- (22) Blaser, H. U.; Steiner, H.; Studer, M. *ChemCatChem* **2009**, *1*, 210.
- (23) Corma, A.; González-Arellano, C.; Iglesias, M.; Sánchez, F. *Appl. Catal. A: Gen.* **2009**, *356*, 99.
- (24) Xu, D.; Liu, Z.; Yang, H.; Liu, Q.; Zhang, J.; Fang, J.; Zou, S.; Sun, K. *Angew. Chem., Int. Ed.* **2009**, *48*, 4217.
- (25) Tang, L.; Han, B.; Persson, K.; Friesen, C.; He, T.; Sieradzki, K.; Ceder, G. *J. Am. Chem. Soc.* **2009**, *132*, 596.
- (26) Matanovic, I.; Garzon, F. H.; Henson, N. J. *J. Phys. Chem. C* **2011**, *115*, 10640.
- (27) Stamenkovic, V. R.; Mun, B. S.; Arenz, M.; Mayrhofer, K. J.; Lucas, C. A.; Wang, G.; Ross, P. N.; Markovic, N. M. *Nat. Mater.* **2007**, *6*, 241.